# Temporal-spatial progress of cartilage nanocalcification in osteoarthritis development

**Xiaozhao Wang**
Zhejiang University
**Qin Wu**
Zhejiang University
**Ru Zhang**
Zhejiang University
**Zhang Fan**
Zhejiang University
**Wenyue Li**
Zhejiang University
**Renwei Mao**
Zhejiang University
**Zihao Du**
Zhejiang University
**Xudong Yao**
Zhejiang University
**Yuanzhu Ma**
Zhejiang University
**Yiyang Yan**
Zhejiang University
**Wei Sun**
Zhejiang University
**Hongwei Wu**
Zhejiang University
**Wei Wei**
Zhejiang University-University of Edinburgh Institute
**Yejun Hu**
Zhejiang University
**Yi Hong**
Zhejiang University
**Huan Hu**
Zhejiang University
**Yi Wen Koh**

Zhejiang University

**Wangping Duan**

Shanxi Medical University

**Hongwei Ouyang** ( hwoy@zju.edu.cn )

Zhejiang University https://orcid.org/0000-0002-0922-4209

---

**Article**

**Keywords:** Cartilage nano-calcification, OA, sandwich structure of calcification, calcium-containing matrix vesicles, osteochondral interface

**Posted Date:** April 6th, 2022

**DOI:** https://doi.org/10.21203/rs.3.rs-1437899/v1



---

# Abstract

While osteoarthritis (OA) involves pathological cartilage calcification, its progress is not fully understood. Here, we investigated the temporal-spatial mechanism of mineral transformation pathways in human OA cartilage tissues via multiple imaging tomography at nanoscale resolution. We found that OA progressed by both top-down calcification at the joint surface and bottom-up calcification at the osteochondral transition zone. The top-down calcification process started with the formation of spherical mineral particles in the joint surface during early-stage OA (OA-E), followed by fiber formation and compact material transformation deep into the cartilage during advanced-stage OA (OA-A). The bottom-up calcification in OA-E started when an excessive layer of calcified tissue formed above the original calcified cartilage; there was a 100–200 μm thick layer of noncalcified cartilage tissues between the original and new calcified layers, forming a sandwich structure at the osteochondral transition zone. The abnormal calcified layer was located at the edge of the tidemark that contained acidic components (-COOH) that can chelate $Ca^{2+}$ and bind with $PO_4^{3-}$ to form crystals. It is likely that this local mineralization process was assisted by nearby hypertrophic chondrocytes. With OA progression, the original and upper layers of calcified cartilage fused, which thickened the calcified cartilage region and disrupted cartilage. During OA-E, the calcified cartilage was hypermineralized and contained stiffer carbonated hydroxyapatite (Hap); during OA-A, it was hypomineralized and contained softer HAp. Distinct mechanisms, such as nucleation on matrix vesicles in OA-E and carbonate cores in OA-A, may be involved. These findings illustrated that the progress of pathological calcification was location-specific at the joint surface and osteochondral interface in the early and advanced stages of OA. It is very important to understand the mechanism of OA progression and develop better strategies for future OA treatment on targeting cartilage pathological calcification


# Introduction

Osteoarthritis (OA) is the most common knee joint disorder and affects over 250 million people worldwide, leading to physical disability.[1] Pathological calcification is an inevitable process that occurs in the cartilage when undergoing joint replacement surgery for severe OA.[2–4] Calcium pyrophosphate dehydrate (CPPD) and basic calcium phosphate (BCP) crystals (including amorphous apatite (ACP), octacalcium phosphate (OCP) and carbonated hydroxyapatite (HAp)) were the main components detected on the cartilage surface.[4,5] It was believed that cartilage calcification is a hallmark of advanced OA.[3,6] However, little is known about the progress of calcification in cartilage during OA development. So far, there is no OA treatments available on preventing cartilage pathological calcification.

Previous studies revealed that minerals formed in the joint surface of OA were associated with transdifferentiated chondrocytes.[5,7,8] The formed minerals, in turn, induced “microcrystal-induced stress” on the surrounding cartilage to play a pathogenic role in OA. It is widely considered that the minerals in cartilage are bioproducts of cartilage degeneration and presumably initiate OA.[3] The minerals form through the molecular processes of nucleation, growth and maturation in vitro and in vivo. However, apart

from being a cellular process, little is known about their initiation and very early formation of mineral nuclei, their subsequent transformation in cartilage lesion sites, and how they progress to OA. Until now, no strategies or drugs have been available to prevent crystal deposition and permit mineral dissolution in OA cartilage.[3,4] There is an urgent need to uncover the underlying calcification mechanism in cartilage, which will help us to better understand the pathogenesis of OA and provide a potential therapeutic target.

The progression of calcified cartilage was also found at the osteochondral transitional zone of OA. [9,10] In this process, cartilage destruction and subchondral bone (SB) remodeling have been extensively studied and are considered synchronous phenomena in OA due to their whole joint disease features. [9,11–13] Thus, the changes in the calcified cartilage, an important connecting layer, were concurrent at the very early stage of OA, even before cartilage loss, which could affect the homeostasis of the whole joint.[14] However, the difficulty in distinguishing thin calcified cartilage from the complex osteochondral interface, due to the limitation in the resolution of the current microscopic imaging methods, is an obstacle in understanding the mechanism associating structural and compositional changes involved in this pathological calcification process of calcified cartilage in OA.[9]

As a result, the temporal and spatial progress of cartilage calcification was not clear in the findings of previous OA research. Thus, high-resolution micro/nanoscale structure elucidation of cartilage calcification at different stages is urgently needed to gain insights into the pathogenesis and progression of OA. Multiple imaging tomography has been applied to study the nanoscale architecture and composition of physiological bones and the calcification processes of pathological calcified cardiovascular tissues and kidney stones.[15–17] In this work, we combined scanning electron microscopy (SEM), transmission electron microscopy (TEM), atomic force microscopy (AFM), and focused ion beam-scanning electron microscopy (FIB-SEM) with high-resolution transmission electron microscopy-electron energy loss spectroscopy (HRTEM-EELS) and investigated the location and stage-specific pathology of calcification and explored their contributing roles in OA initiation and progression.

# Results

**Characterizing calcification on the joint surface during OA development.** Normal samples and cartilage tissues in early-stage OA (OA-E) and advanced-stage OA (OA-A) were collected and carefully identified through different histologic features for further analysis (Fig. S1). Intact surface and superficial fibrillation were mainly present in OA-E samples, while OA-A samples were largely eroded, a large amount of cartilage had been lost. Next, we examined the joint surface by SEM techniques coupled with energy-dispersive X-ray spectroscopy (EDX) to visualize the topographical characteristics and elemental compositions for each group. The normal joint surface demonstrated collagen fiber alignment without mineral deposition in both SEM and density-dependent color (DDC)-SEM micrographs. In contrast, OA-E surfaces showed some thickened collagen fibrils (Fig. 1b), spherical mineral particles (dimensions ranged from 25 nm to 2.1 μm, n = 841) and calcified fibers (Fig. 1e, Fig. 1k, and Fig. S2). Notably, OA-A surfaces had apparent mineral deposition in three distinct forms: spherites (dimensions of 80 nm ~ 2.4 μm, n =

996), calcified fibers, and compact materials (Fig. 1c, 1f and 1l, Fig. S2). In addition to mineral accumulation on the cartilage surface, mineral deposition in deeper cartilage was detected in OA-A samples (Fig. S3).

Moreover, the presence of calcium (Ca), phosphorus (P), and small amounts of magnesium (Mg) and sodium (Na) were revealed by EDX between the OA-E and OA-A samples. There were no significant variations in Ca and P (Fig. 1h and Fig. 1i), while OA-E appeared to have slightly higher Mg content than OA-A. As Mg is a phase stabilizer for mineral precursors but highly unstable in bulk HAp,[18] it is possible that the higher Mg level contributes to the mineral nucleation in OA-E, and lower Mg may be related to spherite growth in OA-A. In addition, we analyzed the Ca/P ratios within minerals with respect to the degree of mineralization.[19] The Ca/P ratios in OA-E cartilage (1.59 ± 0.047) were comparable to those of the mature bone matrix.[20] Meanwhile, the minerals in the OA-A cartilage were large with a wider distribution than those in OA-E cartilage (Fig. 1k and Fig. 1l), which may correspond to lower Mg concentrations. It appears that a larger mineral particle size correlated with greater OA severity. This phenomenon was also demonstrated in the calcified cardiovascular tissues of humans.[21]

Calcified matter was previously identified histologically and radiologically in OA cartilage and is considered an important feature of OA progression.[2,22] However, mechanisms for the formation and progression of calcified matter in OA have never been extensively investigated.[3] We found a large amount of Ca- and P-containing spherites arising at early-stage OA cartilage surfaces. Such spherites appeared to grow larger with different morphologies and even extended to the deeper zones of cartilage in OA-A (Fig. 1h). Such submicron spherical structures have not been examined previously in bone but were discovered in calcified cardiovascular tissues with a diverse range of diseases and in the lacunae micropetrosis in aged bone.[23,24] These mineralized spherites seemed to be an intermediate form of calcified minerals, and it was suggested that they were important building blocks in the formation of the calcified region at lesion sites.[21] The Mg-rich feature of the spherites deposited on the joint surface may suggest their cellular origin given that $Mg^{2+}$ ions were important intracellular ions that were largely concentrated in apoptotic bodies and matrix vesicles.[25,26] The globular apoptotic bodies and matrix vesicles contained biomolecules such as phosphatidylserine,[27] tissue-nonspecific alkaline phosphatase (TNAP)[28] and annexins.[29] which allow $Ca^{2+}$ and phosphate ($PO_4^{3-}$) accumulation and uptake from the surface[26,30]. The accumulation of $Ca^{2+}$ and $PO_4^{3-}$ was reported to mainly surround the chondrocytes in OA[31] and is known to induce chondrocyte hypertrophy that is closely associated with matrix mineralization.[2] Together with the higher content of $Mg^{2+}$, which stabilizes the precursor,[18,32] the accumulation of $Ca^{2+}$ and $PO_4^{3-}$ regulates spherite formation and growth in OA-E. OA cartilage that was found to increase levels of Ca, P and Mg, supporting mineral deposition.[31,33] Thus, cartilage calcification is not a passive deposition of CaP but an early event during OA initiation alongside the phenotypic alterations of chondrocytes.[2,5,34]

**Advancement of calcified matter from calcified cartilage into deep cartilage during OA processes.**
Significant changes in the composition and structure of cartilage and SB have been thoroughly investigated in OA,[11] but those of the connective layer that cause the breakdown of cartilage to predispose OA are unknown. [35] As the invasion of calcified cartilage into the overlying cartilage and duplicated tidemarks are hallmarks of OA,[11] we next focused on the detailed mineral assembly patterns and structural organization involved in pathological calcification in different OA stages. Distinct microstructural units at the osteochondral interface were revealed by histological staining in different OA stages (Fig. 2a). Further study by DDC-SEM was conducted to image and examine the microstructures associated with OA status (Figs. 2b). As a result, normal calcified cartilage showed a gradient of spherical minerals proximal to cartilage (zone-1, active calcified matter formation sites) and densely packed minerals adjacent to SB (zone-2) (Fig. 2c). In OA-E cartilage, we found an obvious 100–200 μm-wide calcified layer invading the overlying original calcified cartilage, forming a sandwich structure at the osteochondral transitional zone (Fig. 2b, 2f). The mineral distribution patterns in OA-E cartilage were largely identical to those of the normal calcified cartilage (Fig. 2c). In contrast, the microstructures of calcified cartilage were completely disrupted in OA-A samples (Figs. 2c). A large number of chondrocytes residing in partially calcified lacunae were localized within the mineralization front region of calcified cartilage tissues in both OA-E and OA-A samples, suggesting that these chondrocytes underwent hypertrophy or apoptosis to contribute to calcifying invasion into cartilage (Fig. S4). The progressive mineralized region (zone-1) at the mineralization front of the interface was the active region for calcified invasion. The subsequent EDX line scan indicated an increased thickness of zone-1 that was predominant in both OA-E and OA-A cartilage, compared with healthy samples (Fig. 2d). This suggests the intrusion of calcification into the overlying cartilage to some extent when OA develops (Fig. S4-S5). The elemental compositions of minerals differed between zone-1 and zone 2 for all samples, accompanied by an increased Ca/P ratio from zone-1 to zone-2 (Fig. 2e). The OA-E samples had a Ca/P ratio similar to that of the healthy control in both zone-1 (1.52 ± 0.23 vs. 1.56 ± 0.12) and zone-2 (1.80 ± 0.10 vs. 1.76 ± 0.08), whereas that of OA-A was slightly lower in both zones compared with the control (1.41 ± 0.12 for zone-1, 1.66 ± 0.16 for zone-2). As the Ca/P ratio is indicative of the mineralization degree,[19] it was suggested that minerals in calcified cartilage exhibited local variations in their assembly patterns during the evolution of OA pathology.

To understand the changes in mineral assemblies that occurred in the OA calcified cartilage, FIB-SEM was applied to map the nanoscale structural details. In contrast to the normal control, OA-E and OA-A cartilage showed thickened gradient mineralized regions (Fig. 2g), consistent with the EDX line scan results (Fig. 2d) and bright field TEM images (Fig. S5). From the mineralization front to the highly mineralized region of calcified cartilage, three typical mineral morphologies within the matrix were visualized for normal samples. The morphologies included isolated spherites with diverse sizes, fibers assembled within collagen, and well-organized compact materials with uniformly distributed voids (Figs. 2g-2i). As predicted, the OA-E samples showed different morphologies in the calcified cartilage. For instance, in the mineralization front region, larger and denser spherites with clear outlines as well as larger spherites in needle-shaped crystals were observed (Fig. 2h). Such spherites were rarely associated

with the collagen matrix and were absent from the normal control. In the highly mineralized region, the densely packed particles and compact materials were shown to have more, larger voids (yellow arrowheads). Such voids were predominantly embedded or located at the peripheries of the particles (Figs. 2h and 2i). These mineral particles, which varied in size and morphology, were discretely distributed at the front of the mineralization region of OA-E (Figs. 2h and 2i). In the OA-A samples, larger spherites with fuzzy peripheries were prominent at the mineralization front, where more numerous and larger voids formed in the surrounding matrix (Fig. 2h). The compact materials possessed smaller but more uniformly distributed voids within the structures in the highly mineralized region (Fig. 2h and 2i). The increasing sizes of voids were associated with OA progression (Figs. 2h-2j). The 3D rendering of typical mineral spherites at the mineralization front of calcified cartilage further illustrated the nanoscale variations in mineral structures in OA (Fig. 2j). The OA-E and OA-A samples lost the fiber morphologies of minerals (Figs. 2h and 2i), which was important to the mineral-extracellular matrix (ECM) assemblies during the mineralization process in bone or other soft-to-hard interfaces.[17,36] Meanwhile, considerable variations in mineral morphologies were found at the mineralization front in OA-E and OA-A compared with normal controls (Fig. 2h-2j), possibly indicating different assembly patterns of mineral formation that subsequently promoted the invasion of calcified matter into cartilage or the thickening of calcified cartilage. The larger and increasing number of pores that emerged in calcified cartilage in OA-E may establish communicating channels to facilitate the transfer of molecules to promote crosstalk between cartilage and SB; the largest ones in OA-A may even allow the extension of vessels from SB to the cartilage region.[9,37,38] Certain physicochemical metastability at the osteochondral interfaces of healthy samples was hypothesized to maintain the ultrastructural organization of mineral deposits associated with the surrounding ECM.[39] It could be altered by activating cellular or molecular processes involved in initiating downstream mineralization events at the mineralization front of the calcified cartilage, resulting in calcified matter invasion from calcified cartilage to the overlying cartilage in OA.[11,37] Such a process commonly raises the possibility for concurrent compositional changes in minerals at the osteochondral transitional zone during OA.[10]

**Hypermineralized and hypomineralized HAp minerals in calcified cartilage in early-stage and advanced-stage OA.** Variations in the assembly patterns of minerals in calcified cartilage prompted us to analyze their detailed compositions at multiple scales during OA development. Using XRD, FTIR and Raman spectroscopy analysis, carbonate-substituted hydroxyapatite (HAp)[10] was detected as the main phase of calcified cartilage for all samples (Fig. S6). HAp was also identified as the main mineral phase of the duplicated “calcified region” in OA-E (Fig. S7). This specific region was formed adjacent to the duplicated tidemarks (Fig. 2, Fig. S7). Acidic components (-COOH) of tidemarks could chelate the supersaturated $Ca^{2+}$ and $PO_4^{3-}$ ions in OA cartilage to form crystals.[40,41] The spatial distribution of HAp across the calcified cartilage was further assessed using Raman spectroscopy. The characteristic bands in the Raman spectra at 961 $cm^{-1}$ ($PO_4^{3-}$ $\nu1$ symmetric stretch) and 1071 $cm^{-1}$ ($CO_3^{2-}$ $\nu1$ in-plane vibrations) were used to visualize the spatial distribution of $PO_4^{3-}$ and $CO_3^{2-}$ of minerals (Fig. 3a and 3b). The ionic substitution ratios ($CO_3^{2-}/PO_4^{3-}$) and crystallinity (full-width at half-maximum (FWHM) of the peak at

961 $cm^{-1}$) of HAp across calcified cartilage were also mapped (Fig. 3c and 3d). A depth-dependent increase in $PO_4^{3-}$ and $CO_3^{2-}$ contents, as well as a concomitant decrease in $CO_3^{2-}$ substitution ratios and FWHM, which inversely indicated mineral crystallinity, created a graded 30 μm-wide region at the mineralization front of calcified cartilage for normal cartilage. In contrast, OA-E samples have higher $PO_4^{3-}$ and $CO_3^{2-}$ contents, thus creating a sharp boundary at the mineralization front. Within the same region, $CO_3^{2-}$ substitution ratios were slightly decreased, while mineral crystallinities were markedly improved compared with normal controls. This indicated a hypermineralized feature of HAp minerals in the calcified cartilage in OA-E.[42] OA-A samples have greatly reduced $PO_4^{3-}$ and $CO_3^{2-}$ contents in calcified cartilage, where significantly higher $CO_3^{2-}$ substitution ratios and lower crystallinities were more predominant, suggesting a hypomineralization phenomenon that is completely inverse to OA-E. A previous study also revealed this trend of HAp in calcified cartilage in OA.[10]

Next, we examined the underlying internal nanoscale compositions and organizations of the minerals. Crystalline domains measuring 2–5 nm progressively enlarged and elongated across the interface until they were completely fused at calcified cartilage of normal samples (Fig. 3e). In OA-E samples, the minerals contained larger crystal size, higher aspect ratio, and higher crystallinity near cartilage. The crystalline aggregates fused precociously before reaching the highly mineralized region, revealing more crystalline-like features of minerals at the mineralization front of OA-E. In contrast, OA-A contained crystalline domains with smaller sizes and lower crystallinity from the mineralized front to the highly mineralized region. These results were in good agreement with the Raman results (Fig. 3a-3d) and further supported the morphological variations of minerals in FIB-SEM. Moreover, minerals in OA-E contained higher contents of Ca and P, whereas those in OA-A were significantly decreased when compared with normal samples (Fig. 3f). As the Ca content determines the Ca/P ratios of minerals, this could explain the higher Ca/P ratios of minerals in OA-E and lower in OA-A (Fig. 3g). These results further revealed the nanoscale hypermineralized and hypomineralized phenomena of minerals in calcified cartilage in OA-E and OA-A cartilage.[10] Combining Raman spectroscopy with electron microscopy, we unveiled the compositional variations of minerals in calcified cartilage on a multilevel scale in OA development. Compared with normal cartilage, the substantial deviations in the spatial compositions of HAp at the active mineralization front of calcified cartilage in OA-E and OA-A were closely associated with the morphological changes (Fig. 2).

Next, the distinct local chemical environment of minerals at the calcified region of different cartilages was further studied using EELS. Four typical mineral particles across the calcified cartilage were selected for detailed analysis. Carbon K edge signals (284 eV − 302 eV) revealed the organic matrix for all samples, and the calcium peak at 348 eV − 352 eV confirmed the mineral compounds (Fig. 3h). We generated maps of Ca signals to visualize their distribution within mineral particles across the calcified cartilage (Fig. 3i). The Ca intensity of minerals gradually increased throughout the calcified cartilage region for all samples. Among them, the Ca intensity of minerals in OA-E was greater in the core. In contrast, OA-A gave a more diffuse, cloudy pattern of Ca distribution within minerals that contained a

fairly low amount of Ca. This result corresponded with the EDX mapping in Fig. 3f. Higher Ca intensity contributed to a higher level of crystal perfection in OA-E; Ca loss, in turn, induced imperfection of crystalline aggregates in OA-A.

The striking variations in carbonate content have been reported to cause mineral formation and growth in physiological bone and pathological calcification in kidney and cardiovascular tissues[15,16,19]. Hence, we further studied the fine structures of the carbon K edge. After performing the multi-Gaussian fitting, a small amount of carbonate (peak C at 290 eV)[16,19] was noticeable in the cores of minerals in calcified cartilage for all samples (Fig. 3h, Fig. S8, Table S2). Consistent with the Raman results, the intensity of carbonate was greater within spherical particles in OA-A and less in OA-E. Recently, the detection of carbonate in the core of bone mineral precursors[19] has led to the postulation that carbonated calcium may act as bioseeds for calcium phosphate formation at the mineralization front of calcified cartilage in OA-A. Moreover, the reduction in mineral crystallinity by carbonate substitution into the lattice[43] explains how the graded crystallinity of minerals in normal samples was altered to undergo hypermineralization and hypomineralization in OA-E and OA-A samples, respectively.

We also detected a small number of carbonyl signals (peak B at 287 eV) from mineral structures in OA-E and OA-A samples (Fig. 3h, Fig. S8). These carbonyl signals seemed to be more intense in minerals in OA-E. Their presence should be ascribed to organic compounds such as osteopontin and TNAP (not limited), which were reported to be highly expressed in OA cartilage and played a role in mediating mineral nucleation and growth.[3,44] Such organic compounds assemble onto the membranes of matrix vesicles to entrap ions ($Ca^{2+}$ and $PO_4^{3-}$) for nucleation and crystal growth.[45] A similar process may occur at the mineralization front of calcified cartilage in OA-E.

Overall, these observations suggested that great variations in mineral particles in calcified cartilage, in terms of morphology and composition for OA-E and OA-A tissues, may be ascribed to different nucleation mechanisms: organic compounds (matrix vesicles) for OA-E and calcium carbonate for OA-A.

**Calcium-containing matrix vesicles secreted by hypertrophic chondrocytes drive two kinds of nucleation in OA development.** To ascertain the abovementioned nucleation process, hypertrophic chondrocytes in lacunae in calcified cartilage were further analyzed using DDC-SEM and FIB-SEM (Fig. 4). DDC-SEM micrographs showed the presence of many dense materials (minerals) around the hypertrophic chondrocytes in OA cartilage (Fig. 4a, Fig. S4 and S9). FIB-SEM images validated their submicron structures and surroundings (Fig. 4b). The hypertrophic chondrocytes in OA-E resided in a confined lacunar region located at a distance from the surrounding mineralized islands, while those in OA-A were closely surrounded by minerals. Hypertrophic chondrocytes in OA-E behaved like osteoblasts by secreting inhibitors (e.g., osteopontin) to keep the closest pericellular matrix free of minerals and release promoters (e.g., TNAP) to remove the inhibitors.[46] Without the inhibition of nucleation, crystallization occurred in the ECM.[20,47] Matrix vesicles containing disordered precursors of CaP were closely associated with this

mineralization process.[20,48,49] Thus, we further examined their presence and features in normal and OA samples.

Calcium phosphate-containing matrix vesicles were observed in the ECM within the lacuna of OA-E (Figs. 4b-4d, Fig. S10). Fewer matrix vesicles were found in the same region in OA-A and were rarely detected in normal samples (Figs. 4b-4d). To examine their phase details, the Ca/P ratios of these vesicles were further calculated, and the values for OA-E and OA-A were 0.53 ± 0.21 and 1.34 ± 0.10, respectively (Fig. 4e). In a previous study, a value of 0.75 was identified in intracellular mineral-containing matrix vesicles to be the precursor for HAp.[20] The polyphosphate-Ca complex at new bone formation sites is known to have a Ca/P ratio of 0.5.[50] Other studies similarly revealed precursors within the ECM to have Ca/P ratios of 1.3.[19,51] In our present study, despite the difference in Ca/P ratios between globular vesicles in OA-E and OA-A, the lower Ca/P ratios indicated their disordered features as precursors. The matrix vesicles also contained multiple organic components, which showed various affinities to trap $Ca^{2+}$ or $PO_4^{3-}$. For example, higher TNAP activity allowed the influx of $PO_4^{3-}$, and annexins, and phosphatidylserine enabled the influx of $Ca^{2+}$.[26,52 49,53] The matrix vesicles in OA-E and OA-A may have different biomolecule compositions and result in different Ca/P ratios. In the extracellular mineralization process, the remnants of these matrix vesicles may support the carbonyl signal detected within minerals by EELS in OA-E (Fig. 3h). In addition to the small amount of carbonyl signal in minerals, the carbonate signals in OA-A were more intense in the cores of minerals due to the carbonate calcium that acts as nucleation sites (Fig. 3h). Furthermore, the enzyme carbonic anhydrase attached to matrix vesicles may help mediate the formation of such bioseeds.[54,55] The concentrations of $Ca^{2+}$ and $PO_4^{3-}$ in OA cartilage tissues increased locally for the supersaturation of crystal growth.[31] Thus, the calcium phosphate-containing matrix vesicles contained different enzymes to dictate two kinds of nucleation processes at calcified cartilage in various OA stages (Fig. 4f).

The hypertrophic chondrocytes at calcified cartilage were activated in OA to initiate mineralization by secreting calcium-containing matrix vesicles to the ECM. In the ECM, nucleation and growth occurred to form carbonated HAp, leading to calcified cartilage thickening. Matrix vesicles equipped with different components drive two kinds of nucleation mechanisms in OA-E and OA-A. Higher carbonate substitutions at phosphate and hydroxide sites mean more crystal defects and fewer crystalline features of minerals in OA-A (Fig. 3). The size of the minerals should depend on the balance between nucleation and growth. More matrix vesicles favor more nuclei formation and induce smaller particle size in OA-E, whereas in OA-A, fewer matrix vesicles favor less nuclei formation, which leads to larger crystal growth due to a local depletion of ions (Fig. 2 and Fig. 4). The surrounding ECM alterations in OA, such as a higher expression of collagen (type I and X) and carboxymethylation of collagens at the calcified cartilage front, further favored crystal deposition and growth in OA development.[3,56]

Interestingly, these two kinds of nucleation mechanisms were found in the early event of mineralization in the human kidney.[16] Several studies have also suggested that matrix vesicles are also associated with pathological calcification, such as atherosclerosis, arteriosclerosis, and tumors.[4,15,57] Chen et al. revealed

that matrix vesicles enriched in human body fluids may initiate ectopic calcifications.[58] Thus, ectopic calcification in human bodies may share a similarity in the early formation events of OA.[59] Concerning cartilage calcifications in OA, we further traced the programed development and the material mechanism at the upper zone of cartilage and the underlying calcified cartilage. Although the pathological calcifications at both sites were likely associated with the transdifferentiated chondrocytes, their surrounding environments were significantly different. The joint surface was closely buffered by synovial fluids that contained inflammatory factors, ions and growth factors, while calcified cartilage may undergo uncoupled crosstalk between the overlying cartilage and underlying SB,[38] implying their potentially different mineralization process.

**Hypermineralized and hypomineralized HAp minerals drive improved and reduced mechanical responses of calcified cartilage tissues in early- and advanced-stage OA.** Fundamental disparities in mineral assembly patterns in calcified cartilage in OA-E and OA-A could further induce varied mechanical responses. We first utilized indentation loading to map the stiffness of the calcified cartilage tissues at the microscale (Fig. 5a-5b). A continuously increased tissue modulus in the range from approximately 2 kPa to 2 GPa was observed over a region of ~ 30 μm in calcified cartilage of normal samples (black arrow), which correlated well with the gradually mineralized features (Fig. 5b).[60] OA-E showed a stiffer region that was over ~ 100 μm in width (white arrow) overlying the original calcified cartilage (black arrow) (Fig. 5b). The stiffnesses of both calcified regions in OA-E samples ranged from 4.9 ± 1.26 kPa to 5 ± 0.95 GPa, which were much higher than those in normal samples. This tissue modulus map at the calcified cartilage region was quite consistent with the microstructures observed in Fig. 2 and Fig. S7 and should be driven by the hypermineralized structures (Fig. 3).[10,61] Conversely, OA-A exhibited decreased tissue moduli ranging from 0.6 ± 0.27 kPa to 0.75 ± 0.31 GPa at a broader region of calcified cartilage, which was largely ascribed to the hypomineralization of minerals (Fig. 3).[10]

AFM analyses were further employed to elucidate the nanoscale mechanical profiles of the less mineralized region (i), intermediate mineralized region (ii) and highly mineralized region (iii) in calcified cartilage (Figs. 5c-5e). As a result, these mineralized regions of normal samples showed increasing tissue stiffness with peaks at 1.07 ± 0.21 GPa, 4.13 ± 2.83 GPa and 5.81 ± 0.33 GPa. In each region, OA-E showed improved tissue stiffness with peaks at 4.68 ± 0.37 GPa, 5.1 ± 0.17 GPa, and 6.5 ± 0.67 GPa, respectively. The broadening in the distribution ranged from 16.87 GPa to 48.23 GPa at both the intermediate and the highly mineralized regions indicated a marked mechanical increment in OA-E, implying their stiffer mineral features. Expectedly, the tissue stiffness of these mineralized regions in OA-A peaked at 1.78 ± 0.75 GPa, 2.17 ± 0.98 GPa, and 2.28 ± 0.12 GPa, was lower than that of normal samples. In addition to the peak values, broader and narrower stiffness distributions were predominant in OA-E and OA-A, respectively, and they were largely distinct from the heterogeneity of normal samples that changed from a narrow peak to a broad peak.

The nanoscale mechanical profiles (Figs. 5c-5e) were consistent with the microscale mechanical response of calcified tissues in different OA stages (Figs. 5a-5b). Given that the degree of mineralization

and tissue stiffness are intercorrelated,[42] their considerable increase and decrease in tissue stiffness were due to the hypermineralized and hypomineralized features of minerals in OA-E and OA-A, respectively.[10] A recent study reported that ossification of calcified cartilage could induce a stiffened interface in early-stage OA.[61] Calcified cartilage with stiffer features lacks mechanical nanoheterogeneity in the longitudinal direction for normal joints. This is thought to result in a higher localized stress concentration that leads to a deficiency in force transfer and, consequently, microcracks as an early event in OA-E.[62,63] Such microcracks subsequently propagated into SB plates and elevated cartilage-bone crosstalk.[37] In this process, inflammatory cytokines or growth factors from SB that are detrimental to healthy chondrocytes may diffuse into the overlying cartilage and disrupt cartilage homeostasis.[12] Great number of voids generating channels at the calcified cartilage in OA-E further favored this process (Fig. 2).

As skeletal tissue, cartilage is challenged by mechanical loading from the diarthrodial joints and counterforces from the underlying SB. Anomalous loading commonly leads to cartilage degeneration in OA.[64,65] SB tissues undergo coordinated remodeling to adapt to mechanical stress and in turn exert dynamic effects on the overlying cartilage.[38] In this context, as their connective layer, calcified cartilage should play a role in affecting SB remodeling during OA pathogenesis. In OA-E, a higher mechanical response of calcified cartilage could reduce excessive mechanical loads on adjacent SB, which activates osteoclastic bone resorption of SB. In OA-A, the lower mechanical properties of calcified cartilage induced higher mechanical stress in SB, where osteoblastic bone formation was largely improved.[38] Thus, SB tissues showed bone loss in OA-E and bone sclerosis in OA-A through remodeling.[66] Our nanoscale dissection of the intrusion of calcified cartilage has provided novel insights into the macroscale features in OA and further understanding of the pathogenesis of OA from the perspective of materials science.

# Discussion

Here, we identified a new paradigm for cartilage calcification in OA development (Fig. 6). The spatial-temporal program of both top-down and bottom-up calcification at the joint surface and osteo-chondral transition were illustrated in OA development. During the process of calcification, nanospherical particles deposited at the joint surface cartilage and progressively transformed to become fibers and compact deposits of materials and even invaded into deeper cartilage zones. The hypermineralized minerals formed at the tidemark progressively altered into hypomineralized minerals and invaded upward. Such alteration of mineral assembly patterns led to increased and decreased mechanical responses of the calcified tissues at OA-E and OA-A, respectively. This process not only transfers aberrant mechanical force to the overlying cartilage to affect cartilage homeostasis but also releases abnormal mechanical stress to the underlying SB, where bone remodeling is coordinately mediated.[4,9,11,38]

Nanospherites form first at the lesion sites of joint surface cartilage and then generate “crystal-induced stress” to trigger phenotypic changes in chondrocytes, which subsequently drive mineralization events and mediate the formation of compact materials.[57] This process resembled the outcome of CaP

implantation in nonbone tissues to stimulate bone formation.[67,68] This further implied the interplay between cell mediation and mineral formation in ectopic calcifications within soft tissues. As a load-bearing tissue, the chondrocytes in cartilage are sensitive to mechanical stress. Our previous study showed that a stiffer mechanical environment could induce hypertrophy of chondrocytes.[69] Other studies also demonstrated that stiffer substrates could drive the differentiation of stem cells toward an osteoblast-like phenotype.[70] This may further explain the transdifferentiation of chondrocytes around spherites, as they were largely stiffer than the surrounding ECM matrix. In addition, the imbalance between mineralization inhibitors and promoters contributes to mineral formation. For example, as the hallmark of OA, the loss and clearage of proteoglycans released inhibitory effects for mineralization, and upregulated expression of collagen-I promoted calcification.[3,59] The inflammation caused by crystals further adds to the mineralization of cartilage through a cell-mediated process.[4,71,72] In this mineralization-promoted environment, the mineral-containing matrix vesicles[73] or apoptotic bodies[74] released by hypertrophic/apoptotic chondrocytes could spread into the ECM, where higher concentrations of $Ca^{2+}$ and $PO_4^{3-}$ in OA cartilage[31] supported mineral nucleation from the template and further growth (Fig. 6).[8,49] The transformation in the morphology of minerals in cartilage was similar to the sequential morphological transformations for CaP mineralization in vitro and in vivo.[19,48,75] Combined with the fact that HAp was the predominant crystal phase deposited in the calcified cartilage, these findings suggest that the pathological mineralization occurring in OA cartilage could be identical to the physiological process in bone.[3,4] Although CPPD and BCP crystals were reported to coexist during cartilage calcification in OA,[3,4] we detected only the latter phase in this study, which could be due to the limited sample size. This was considered a limitation of this study.

The bottom-up invasion of the calcified cartilage at the tidemark toward the overlying cartilage also played a role in initiating and/or accelerating OA. However, its exact role and material mechanisms are still poorly understood. Previous studies identified tidemark duplication and calcified cartilage thickening at calcified cartilage as OA hallmarks.[10,61] Using high-resolution materials science technology, we revealed the microscale and nanoscale structural and compositional changes in calcified cartilage and their mechanisms during OA progression. The hypermineralized and hypomineralized HAp minerals were enhanced in OA-E and OA-A, respectively (Fig. 3), which could be due to two kinds of nucleation processes of minerals (Fig. 4). It was suggested that the calcium-containing matrix vesicles and calcium carbonate acted as bioseeds for mineral deposition in OA-E and OA-A. Both nucleation processes were demonstrated previously at the cell and tissue levels. [16,19,20,48,52] The different nucleation processes regulated by hypertrophic chondrocytes in calcified cartilage contributed to the distinct mineral assembly patterns, leading to increased and decreased mechanical responses of calcified cartilage tissues.

An extended layer of cartilage calcification is an important feature in OA-E, yet its progression and function in mediating calcified cartilage intrusion in OA are poorly understood. We observed an obvious sandwich structure that consisted of two layers of calcified tissues separated by a 100–200 μm thick layer of cartilage tissue (Fig. 2, Fig. S7). The precise composition of the tidemark was not clear; we knew

only that it contained many acidic components including DNA (basophilic line in histological staining).[76] The acidic molecules could template mineralization via chelating $Ca^{2+}$ and and $PO_4^{3-}$ ions to form crystals.[40,77] The nearby hypertrophic chondrocytes should further assist this local mineralization process by secreting mineralization promoters (Fig. 6). With OA progression, the fusing of the original calcified cartilage with the duplicated calcified region contributed to calcified cartilage thickening and cartilage disruption. A deeper understanding of the processes at the unique calcified cartilage may provide insights for the future treatment of OA.[35]

Thus, we examined the stage- and location-specific calcification process in OA development. Pathological calcification within both zones during the very early events of OA were closely associated with the terminal differentiation and hypertrophy of chondrocytes. Traditional drugs used to prevent crystal deposition in cartilage, including phosphocitrate and sodium thiosulfate, often have limited results due to the uncertain and inaccurate timing and target of the drug effects.[3,4] Based on the new cartilage calcification mechanism during OA development, new treatments on preventing pathological calcification can be developed in future. Controlling the start of pathological calcification could be a potential target for OA treatment. For the top-down calcification at joint surface, methods to prevent the initial formation and growth of HAp by suppressing the trans-differentiation of chondrocytes and reducing the concentration of $Ca^{2+}$ and $PO_4^{3-}$ ions in synovial fluid could be developed. As for the bottom-up cartilage calcification at the osteochondral transition zone, therapeutic strategies to regulate cell metabolism activities need to be developed. Given the complexity of this disease, there may be a large subset of OA cases associated with pathological calcification[3,4,78] that will need further scrutiny in future studies.

# Declarations


## Acknowledgements

We thank Nianhang Rong for the SEM imaging and EDX analysis; we thank Guoqing Zhu for the HRTEM and SAED imaging; we thank Mr. Jiansheng Guo for the FIB-SEM imaging and analysis. This work was supported by the National Key R&D Program of China (2017YFA0104900), the National Science Foundation of China (NO. T2121004, 31830029, 82002271, 81902187).


## Author contributions

X.W., Q.W., and R.Z contributed equally for this work. X.W. and H.O. conceived the project; X.W., Q.W., Z.F., W.L., Z.D. and R.M. carried out the experiments; Z.F. and R.Z. performed the 3D rendering of FIB-SEM; Q.W. and Z.F. performed the histological staining and nanoindentation test; Y.H. analyzed the mechanical response; X.W. and H.O. wrote the manuscript; all authors commented on the manuscript.

## Additional information

All data are available in the manuscript or the supplementary materials.

### Competing financial interests

The authors declare no competing financial interests.

### Additional information

Extended data is available for this paper at

Supplementary information is available for this paper at

# References


1. Murray CJ, Vos T, Lozano R, Naghavi M, Flaxman AD, Michaud C et al (2012) Disability-adjusted life years (DALYs) for 291 diseases and injuries in 21 regions: a systematic analysis for the Global Burden of Disease Study 2010. Lancet 380:2197–2223
2. Fuerst M, Bertrand J, Lammers L, Dreier R, Echtermeyer F, Nitschke Y et al (2009) Calcification of articular cartilage in human osteoarthritis. Arthritis Rheum 60:2694–2703
3. Yan JF, Qin WP, Xiao BC, Wan QQ, Tay FR, Niu LN et al (2020) Pathological calcification in osteoarthritis: an outcome or a disease initiator? Biol Rev Cambridge Philos Soc 95:960–985
4. McCarthy GM, Dunne AJ (2018) N. r. R. Calcium crystal deposition diseases-beyond gout. Nat Rev Rheumatol 14:592–602
5. Ea H-K, Nguyen C, Bazin D, Bianchi A, Guicheux J, Reboul P et al (2011) Articular cartilage calcification in osteoarthritis: Insights into crystal-induced stress. Arthritis Rheum 63:10–18
6. McCarthy GM, Cheung HS (2009) J. C. r. r. Point: Hydroxyapatite crystal deposition is intimately involved in the pathogenesis and progression of human osteoarthritis. Curr Rheumatol Rep 11:141–147
7. van der Kraan PM, van den Berg WB (2012) Chondrocyte hypertrophy and osteoarthritis: role in initiation and progression of cartilage degeneration? Osteoarthr Cartil 20:223–232
8. Thouverey C, Bechkoff G, Pikula S, Buchet RJ (2009) O. Inorganic pyrophosphate as a regulator of hydroxyapatite or calcium pyrophosphate dihydrate mineral deposition by matrix vesicles. Osteoarthritis Cartilage 17:64–72
9. Burr DB, Gallant MA (2012) Bone remodelling in osteoarthritis. Nat Rev Rheumatol 8:665–673
10. Das Gupta S, Finnila MAJ, Karhula SS, Kauppinen S, Joukainen A, Kroger H et al (2020) Raman microspectroscopic analysis of the tissue-specific composition of the human osteochondral junction in osteoarthritis: A pilot study. Acta Biomater 106:145–155
11. Goldring SR, Goldring MB (2016) Changes in the osteochondral unit during osteoarthritis: structure, function and cartilage-bone crosstalk. Nat Rev Rheumatol 12:632–644
12. Goldring MB, Goldring SR (2010) Articular cartilage and subchondral bone in the pathogenesis of osteoarthritis. Ann N Y Acad Sci 1192:230–237

13. Burr DB, Gallant MA (2012) Bone remodelling in osteoarthritis. Nat Rev Rheumatol 8:665–673
14. Lories RJ, Luyten FP (2011) The bone-cartilage unit in osteoarthritis. Nat Rev Rheumatol 7:43–49
15. Bertazzo S, Gentleman E, Cloyd KL, Chester AH, Yacoub MH, Stevens M (2013) M. Nano-analytical electron microscopy reveals fundamental insights into human cardiovascular tissue calcification. Nat Mater 12:576–583
16. Gay C, Letavernier E, Verpont M-C, Walls M, Bazin D, Daudon M et al (2020) Nanoscale analysis of Randall's plaques by electron energy loss spectromicroscopy: insight in early biomineral formation in human kidney. ACS Nano 14:1823–1836
17. Reznikov N, Bilton M, Lari L, Stevens MM, Kröger RJ (2018) Fractal-like hierarchical organization of bone begins at the nanoscale. Science 360:6388–6397
18. Salimi M, Heughebaert J, Nancollas GJ (1985) L. Crystal growth of calcium phosphates in the presence of magnesium ions. Langmuir 1:119–122
19. Nitiputri K, Ramasse QM, Autefage H, McGilvery CM, Boonrungsiman S, Evans ND et al (2016) Nanoanalytical electron microscopy reveals a sequential mineralization process involving carbonate-containing amorphous precursors. ACS Nano 10:6826–6835
20. Mahamid J, Sharir A, Gur D, Zelzer E, Addadi L, Weiner S (2011) Bone mineralization proceeds through intracellular calcium phosphate loaded vesicles: a cryo-electron microscopy study. J Struct Biol 174:527–535
21. Bertazzo S, Gentleman E, Cloyd KL, Chester AH, Yacoub MH, Stevens M (2013) M. Nano-analytical electron microscopy reveals fundamental insights into human cardiovascular tissue calcification. Nat Mater 12:576–583
22. Hubert J, Beil F, Rolvien T, Butscheidt S, Hischke S, Püschel K et al (2020) Cartilage calcification is associated with histological degeneration of the knee joint: a highly prevalent, age-independent systemic process. Osteoarthritis Cartilage 28:1351–1361
23. Bertazzo S, Steele JAM, Chester AH, Yacoub MH, Stevens MM (2014) Cardiovascular calcification violet pearl. Lancet 384:9950
24. Milovanovic P, Zimmermann EA, Vom Scheidt A, Hoffmann B, Sarau G, Yorgan T et al (2017) The formation of calcified nanospherites during micropetrosis represents a unique mineralization mechanism in aged human bone. Small 13:1602215–1602224
25. Fernández-Segura E, Canizares FJ, Cubero MA, Warley A, Campos AJ (1999) E. c. r. Changes in elemental content during apoptotic cell death studied by electron probe X-ray microanalysis. Exp Cell Res 253:454–462
26. Wuthier RE, Lipscomb GFJFB (2011) Matrix vesicles: structure, composition, formation and function in calcification. Front Biosci 16:2812–2902
27. Mariño G, Kroemer GJ (2013) C. r. Mechanisms of apoptotic phosphatidylserine exposure. Cell Res 23:1247–1248

28. Ali SY (1976) Analysis of matrix vesicles and their role in the calcification of epiphyseal cartilage. *Fed. Proc.* **35**, 135–142
29. Golub EE (2009) J. B. e. B. A.-G. S. Role of matrix vesicles in biomineralization. Biochim Biophys Acta Gen Subj 1790:1592–1598
30. Reynolds JL, Joannides AJ, Skepper JN, McNair R, Schurgers LJ, Proudfoot D et al (2004) Human vascular smooth muscle cells undergo vesicle-mediated calcification in response to changes in extracellular calcium and phosphate concentrations: a potential mechanism for accelerated vascular calcification in ESRD. J Am Soc Nephrol 15:2857–2867
31. Cillero-Pastor B, Eijkel G, Kiss A, Blanco FJ, Heeren RM (2012) J. A. c. Time-of-flight secondary ion mass spectrometry-based molecular distribution distinguishing healthy and osteoarthritic human cartilage. Anal Chem 84:8909–8916
32. Roschger A, Wagermaier W, Gamsjaeger S, Hassler N, Schmidt I, Blouin S et al (2020) Newly formed and remodeled human bone exhibits differences in the mineralization process. Acta Biomater 104:221–230
33. Pritzker KP, Châteauvert JM, Grynpas MD (1987) Osteoarthritic cartilage contains increased calcium, magnesium and phosphorus. J Rheumatol 14:806–810
34. Pitsillides AA, Beier F (2011) Cartilage biology in osteoarthritis-lessons from developmental biology. Nat Rev Rheumatol 7:654–663
35. Nukavarapu SP, Dorcemus DL (2013) Osteochondral tissue engineering: current strategies and challenges. Biotechnol Adv 31:706–721
36. Wang X (2022) Identification of an ultrathin osteochondral interface tissue with specific nanostructure at the human knee joint. Nano Lett. doi.org/10.1021/acs.nanolett.1c04649. Lin J., Li Z., Ma Y., Zhang X., He Q., Wu Q., Yan Y., Wei W., Yao X., Li C., Li W., Xie S., Hu Y., Zhang S., Hong Y., Li X., Chen W., Duan W., Ouyang H
37. Pan J, Wang B, Li W, Zhou X, Scherr T, Yang Y et al (2012) Elevated cross-talk between subchondral bone and cartilage in osteoarthritic joints. Bone 51:212–217
38. Hu W, Chen Y, Dou C, Dong SJ (2021) A. o. t. R. D. Microenvironment in subchondral bone: predominant regulator for the treatment of osteoarthritis. Ann Rheum Dis 80:413–422
39. Zou Z, Tang T, Macias-Sanchez E, Sviben S, Landis WJ, Bertinetti L, Three-dimensional structural interrelations between cells, extracellular matrix, and mineral in normally mineralizing avian leg tendon. *Proc. Natl. Acad. Sci.* **117**, 14102–14109 et al (2020)
40. Lyons T, Stoddart R, McClure S, McClure JJ (2005) The tidemark of the chondro-osseous junction of the normal human knee joint. J Mol Histol 36:207–215
41. Yoreo JJD, Gilbert PUPA, Sommerdijk NAJM, Penn RL, Whitelam S, Joester D et al (2015) Crystallization by particle attachment in synthetic, biogenic, and geologic environments. Science 349:6247–6256
42. Gupta HS, Schratter S, Tesch W, Roschger P, Berzlanovich A, Schoeberl T et al (2005) Two different correlations between nanoindentation modulus and mineral content in the bone–cartilage interface.

J Structur Biol 149:138–148

43. Wingender B, Azuma M, Krywka C, Zaslansky P, Boyle J, Deymier A (2021) J. A. b. Carbonate substitution significantly affects the structure and mechanics of carbonated apatites. Acta Biomater 122:377–386
44. Reznikov N, Steele JAM, Fratzl P, Stevens M (2016) M. A materials science vision of extracellular matrix mineralization. Nat Rev Mater 1:1–14
45. Nudelman F, Pieterse K, George A, Bomans PHH, Friedrich H, Brylka LJ, The role of collagen in bone apatite formation in the presence of hydroxyapatite nucleation inhibitors. *Nat. Mater.s* **9**, 1004–1009 et al (2010)
46. Reznikov N, Hoac B, Buss D, Addison W, Barros N, McKee MJ (2020) B. Biological stenciling of mineralization in the skeleton: Local enzymatic removal of inhibitors in the extracellular matrix. Bone 138:115447
47. Ayoubi M, van Tol AF, Weinkamer R, Roschger P, Brugger PC, Berzlanovich A et al (2021) 3D interrelationship between osteocyte network and forming mineral during human bone remodeling. Adv Healthc Mater 10:2100113–2100123
48. Boonrungsiman S, Gentleman E, Carzaniga R, Evans ND, McComb DW, Porter AE, The role of intracellular calcium phosphate in osteoblast-mediated bone apatite formation. *Proc. Natl. Acad. Sci.* **109**, 14170–14175 et al (2012)
49. Bottini M, Mebarek S, Anderson KL, Strzelecka-Kiliszek A, Bozycki L, Simão AMS et al (2018) Matrix vesicles from chondrocytes and osteoblasts: Their biogenesis, properties, functions and biomimetic models. Biochim Biophys Acta Gen Subj 1862:532–546
50. Omelon S, Georgiou J, Henneman ZJ, Wise LM, Sukhu B, Hunt T et al (2009) Control of Vertebrate Skeletal Mineralization by Polyphosphates. PLoS ONE 4:5634–5649
51. Mahamid J, Sharir A, Addadi L, Weiner S (2008) J. P. o. t. N. A. o. S. Amorphous calcium phosphate is a major component of the forming fin bones of zebrafish: Indications for an amorphous precursor phase. JACS 105:12748–12753
52. Anderson HC, Mulhall D, Garimella RJ (2010) L. i. Role of extracellular membrane vesicles in the pathogenesis of various diseases, including cancer, renal diseases, atherosclerosis, and arthritis. Lab Invest 90:1549–1557
53. van de Lest CHA, Vaandrager AB (2007) Mechanism of cell-mediated mineralization. Curr Opin Ortho 18:434–443
54. Müller WE, Schröder HC, Schlossmacher U, Grebenjuk VA, Ushijima H, Wang XJ (2013) B. Induction of carbonic anhydrase in SaOS-2 cells, exposed to bicarbonate and consequences for calcium phosphate crystal formation. Biomaterials 34:8671–8680
55. Stechschulte DJ Jr, Morris DC, Silverton SF, Anderson HC, Väänänen HK (1992) J. B., mineral. Presence and specific concentration of carbonic anhydrase II in matrix vesicles. Bone Min 17:187–191

56. Schwab W, Friess U, Hempel U, Schulze E, Makita Z, Kasper M et al (2002) Immunohistochemical demonstration of N -(carboxymethyl) lysine protein adducts in normal and osteoarthritic cartilage. Histochem Cell Biol 117:541–546
57. Bazin D, Daudon M, Combes C, Rey C (2012) Characterization and Some Physicochemical Aspects of Pathological Microcalcifications. Chem Rev 112:5092–5120
58. Wu C-Y, Martel J, Cheng W-Y, He C-C, Ojcius DM, Young JD (2013) Membrane Vesicles Nucleate Mineralo-organic Nanoparticles and Induce Carbonate Apatite Precipitation in Human Body Fluids. J Biol Chem 288:30571–30584
59. Kirsch TJ (2006) C. o. i. r. Determinants of pathological mineralization. Curr Opin Rheumatol 18:174–180
60. Mente P, Lewis JJ (1994) J. o. O. R. Elastic modulus of calcified cartilage is an order of magnitude less than that of subchondral bone. J Orthop Res 12:637–647
61. Zhang J, Liao L, Zhu J, Wan X, Xie M, Zhang H et al (2018) Osteochondral Interface Stiffening in Mandibular Condylar Osteoarthritis. J Dent Res 97:563–570
62. Madi K, Staines KA, Bay BK, Javaheri B, Geng H, Bodey AJ et al (2020) In situ characterization of nanoscale strains in loaded whole joints via synchrotron X-ray tomography. Nat Biomed Eng 4:343–354
63. Muir P, McCarthy J, Radtke CL, Markel MD, Santschi EM, Scollay MC et al (2006) Role of endochondral ossification of articular cartilage and functional adaptation of the subchondral plate in the development of fatigue microcracking of joints. Bone 38:342–349
64. Zhen G, Guo Q, Li Y, Wu C, Zhu S, Wang R et al (2021) Mechanical stress determines the configuration of TGFbeta activation in articular cartilage. Nat Commun 12:1706
65. Griffin TM, Guilak F (2005) The role of mechanical loading in the onset and progression of osteoarthritis. Exerc Sport Sci Rev 33:195–200
66. Li G, Yin J, Gao J, Cheng TS, Pavlos NJ, Zhang C et al (2013) Subchondral bone in osteoarthritis: insight into risk factors and microstructural changes. Arthritis Res Ther 15:1–12
67. Le Nihouannen D, Daculsi G, Saffarzadeh A, Gauthier O, Delplace S, Pilet P et al (2005) Ectopic bone formation by microporous calcium phosphate ceramic particles in sheep muscles. Bone 36:1086–1093
68. Yuan H, Fernandes H, Habibovic P, De Boer J, Barradas AM, De Ruiter A, Osteoinductive ceramics as a synthetic alternative to autologous bone grafting. *Proc. Natl. Acad. Sci.* **107**, 13614–13619 et al (2010)
69. Zhang X, Cai D, Zhou F, Yu J, Wu X, Yu D et al (2020) Targeting downstream subcellular YAP activity as a function of matrix stiffness with Verteporfin-encapsulated chitosan microsphere attenuates osteoarthritis. Biomaterials 232:119724
70. Lv H, Li L, Sun M, Zhang Y, Chen L, Rong Y et al (2015) Mechanism of regulation of stem cell differentiation by matrix stiffness. Stem Cell Res Ther 6:103

71. Cunningham CC, Mills E, Mielke LA, O'Farrell LK, Lavelle E, Mori A et al (2012) Osteoarthritis-associated basic calcium phosphate crystals induce pro-inflammatory cytokines and damage-associated molecules via activation of Syk and PI3 kinase. Clin Immunol 144:228–236
72. Corr EM, Cunningham CC, Helbert L, McCarthy GM, Dunne AJ (2017) Osteoarthritis-associated basic calcium phosphate crystals activate membrane proximal kinases in human innate immune cells. Arthritis Res Ther 19:1–13
73. Kirsch T, Swoboda B, Nah HD (2000) Activation of annexin II and V expression, terminal differentiation, mineralization and apoptosis in human osteoarthritic cartilage. Osteoarthritis Cartilage 8:294–302
74. Rutsch F, Terkeltaub RJJBS (2005) Deficiencies of physiologic calcification inhibitors and low-grade inflammation in arterial calcification: lessons for cartilage calcification. Jt Bone Spine 72:110–118
75. Wang X, Yang J, Andrei CM, Soleymani L, Grandfield K (2018) Biomineralization of calcium phosphate revealed by in situ liquid-phase electron microscopy. Commun Chem 1:80
76. Simkin PA (2008) A biography of the chondrocyte. Ann Rheum Dis 67:1064–1068
77. Wu S, Zhang M, Song J, Weber S, Liu X, Fan C, Wu Y (2020) Fine customization of calcium phosphate nanostructures with site-specific modification by DNA templated mineralization. ACS Nano 15:1555–1565
78. Yuan C, Pan Z, Zhao K, Li J, Sheng Z, Yao X et al (2020) Classification of four distinct osteoarthritis subtypes with a knee joint tissue transcriptome atlas. Bone Res 8:1–10

# Figures

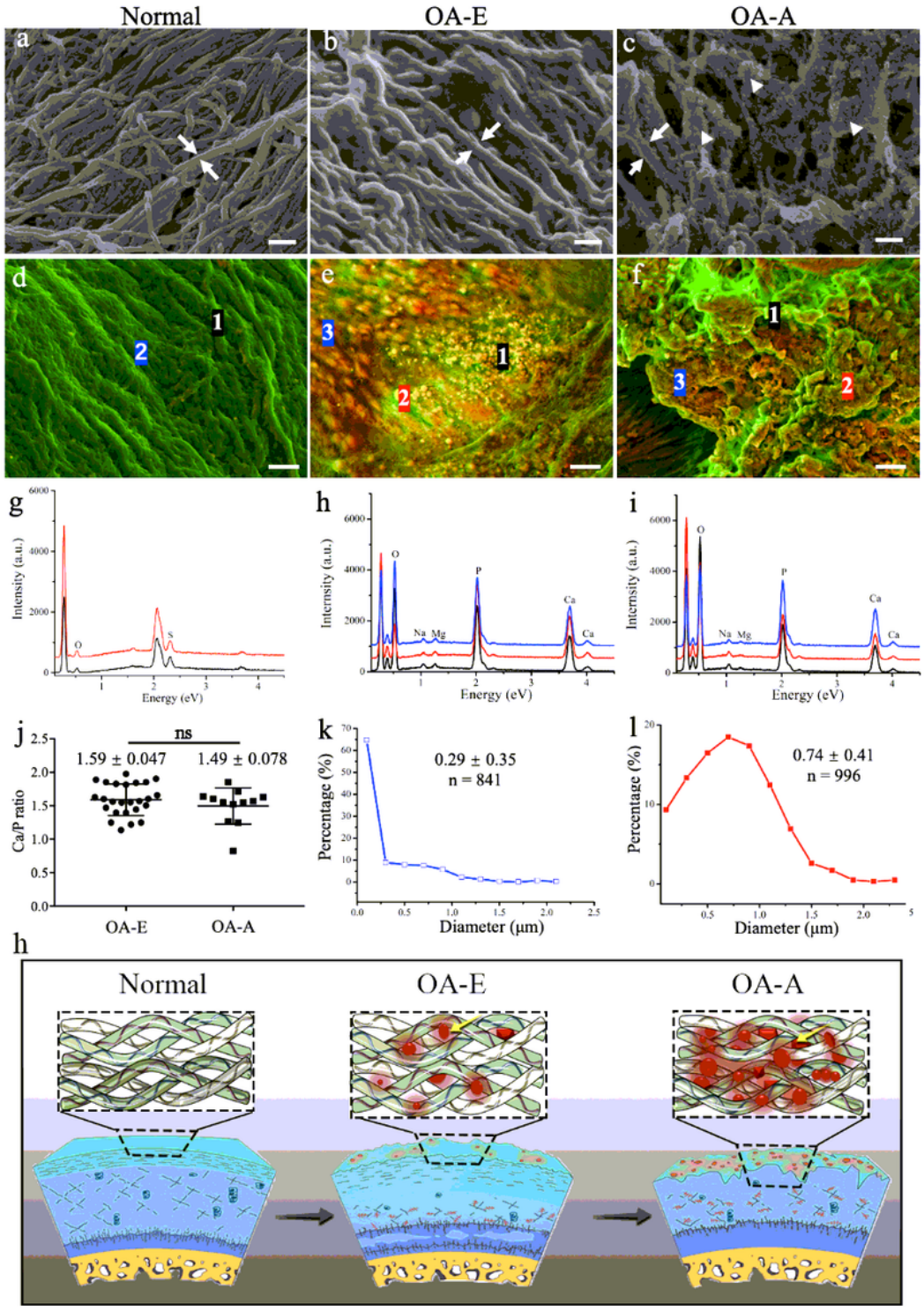


## Figure 1

**Micrographs and elemental analyses of mineral structures identified on normal and different stages of OA cartilage surfaces**. (a-c). SEM micrographs of different cartilage surfaces. (d-f). DDC-SEM micrographs of cartilage surfaces presenting different mineral morphologies, micrographs were colored in post-processing by combining images acquired by backscatter electron and secondary detectors (original images were in Supplementary Fig. S2). Normal cartilage surfaces are mainly aligned collagen

fibers (green), while spherical particles, dense fibers and compact dense materials (red) are predominant on the surface of OA-E and OA-A cartilages. (g-i). Corresponding EDX spectra of the numbered sites in d-f, revealing the chemical composition of minerals on normal, OA-E and OA-A cartilage surfaces. OA-E showed a slightly higher amount of Mg within minerals. (j). The calculated Ca/P ratios of minerals on the surfaces of OA-E and OA-A cartilage. No significant difference (ns) in Ca/P ratios between OA-E and OA-A cartilages. (k, l). Histogram of the average size of mineral particles distributed on OA-E and OA-A cartilage surfaces. (m). Schematic showing calcified matters deposition on joint surface in OA development. Scale bar in a-c, 200 nm, in d-f, 5 μm.

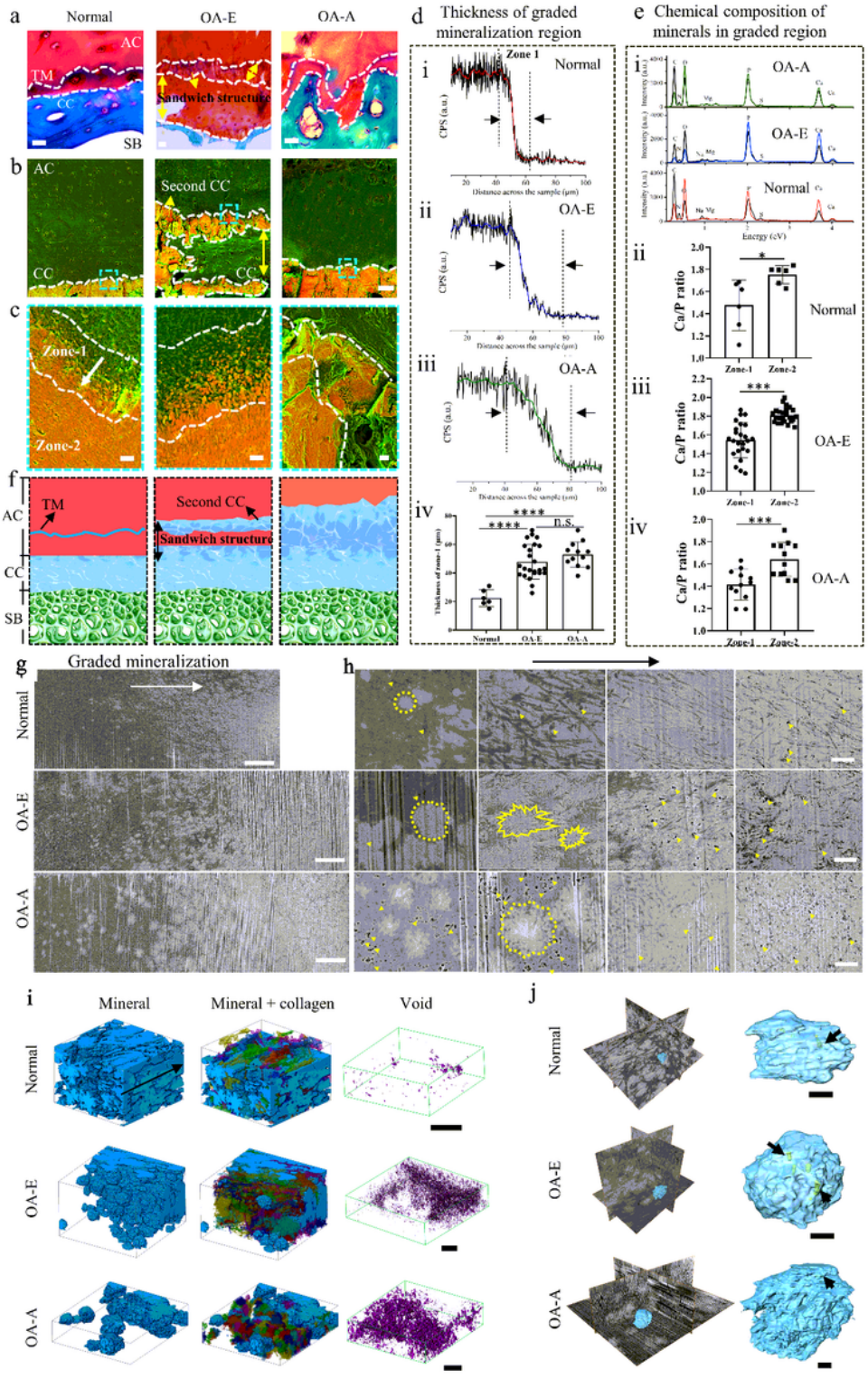


## Figure 2

**Advancement of calcified cartilage into the overlying cartilage as OA processes. (a)**. Histological staining images showing osteochondral features of normal, OA-E and OA-A cartilages. The dotted lines highlighted the tidemark and the front of the calcified cartilage tissues. **(b).** DDC-SEM micrographs of calcified cartilages tissues of normal, OA-E and OA-A samples, respectively. The cartilage tissues were illustrated in green and the calcified cartilage tissues were in orange. The duplicated calcified region with

larger density was obvious, corresponding with histological staining results in (b). **(c)**. The enlarged DDC-SEM micrographs of the progressive mineralized region of different samples. **(d).** The corresponding EDX line scan showing Ca distribution at calcified cartilage (i-iii). Exponential increment regions were calculated as the thickness of zone-1. p value < 0.0001 (****). (iv) in 2d showed the thickness of zone-1 for different samples. **(e)**. Chemical composition of minerals in zone-1 and zone-2. The corresponding Ca/P ratios of minerals within each zone for different samples also calculated (ii-iv). p value for Normal samples = 0.019 (*), p value for OA-E and OA-A < 0.001 (***). **(f).** Schematic diagram displaying the microstructure changes of osteochondral transitional zone as OA processes. AC: articular cartilage, CC: calcified cartilage, SB: subchondral bone, TM: tidemark. **(g).** FIB-SEM images revealing the evolution of morphologies, distributions, and assemblies of mineral particles at calcified cartilage in OA. **(h).** The enlarged BSE images showing multiple minerals with various morphologies dispersed in the matrix. **(i).** 3D rendering of the mineralization front of calcified cartilage showing distinct mineral assembling patterns and void distribution for different samples. **(j).** 3D rendering of typical mineral particles intersecting with three orthogonal FIB-SEM image planes at the mineralization front of interface region, demonstrating the mineral appearance and interior structures under pathological condition (top). The 3D reconstruction of the mineral spherites (cyan) and the fine pores (green, arrows) within minerals delineating the channel-like structures within the mineral (bottom). Scale bars, in a-b = 100 μm, in c = 5μm, in g= 5 μm, in h and i =1 μm; in j= 200 nm.

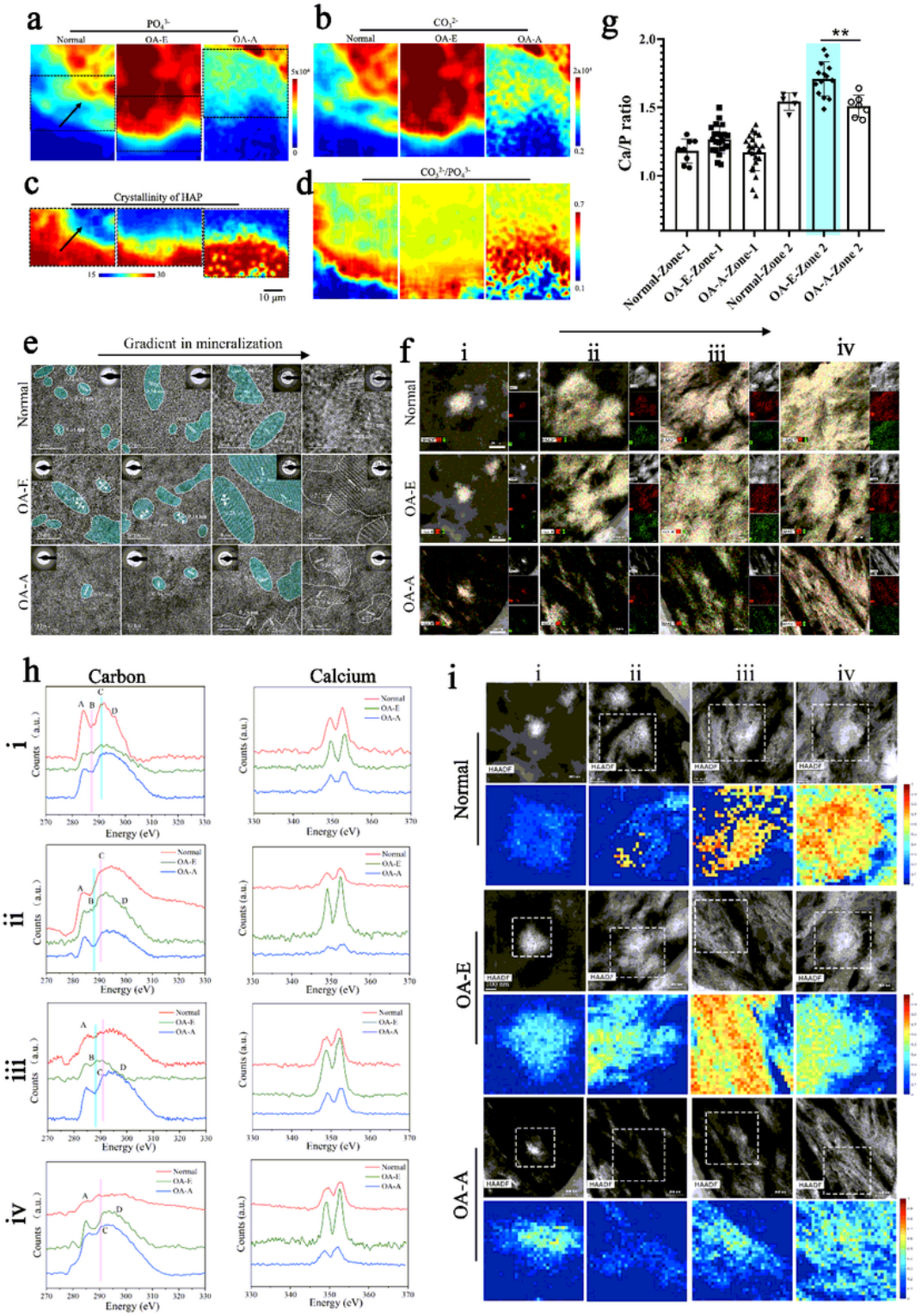


## Figure 3

**Chemical analysis revealing hyper-mineralization in early-stage OA and hypo-mineralization of HAp particles in advanced-stage of OA at calcified cartilage. (a-d).** Collected Raman maps showing HAp contents (960 $cm^{-1}$), $CO_3^{2-}$ substitution (1071 $cm^{-1}$), mineral crystallinity (FWHM of peak 960 $cm^{-1}$), and $CO_3^{2-}/PO_4^{3}$ ratios revealing ionic substitution of minerals across the interface for different samples.

Spatial resolution was 1 μm. **(e).** HRTEM and SAED images revealing mineral assemblies and their crystallinities at calcified cartilage of different samples. **(f).** EDX mapping of Ca and P of the corresponding mineral particles calcified cartilage. **(g).** Ca/P ratios of minerals (calculated by TEM-EDX) distributed at different zones of the calcified cartilage for normal, OA-E and OA-A cartilage samples, respectively. p value = 0.004 (**). **(h).** EELS spectra taken at C-K edge and Ca-$L_{2,3}$ edge collected from different mineral particles (i-iv) of different cartilage samples. **(i).** HHADF-STEM images and corresponding chemical heatmap collected at calcium-$L_{2,3}$ edge of HAp minerals across the interface region for normal, OA-E and OA-A samples. The calcium $L_{2,3}$ edge intensities were integrated over a 50 eV window above the edge onset after background subtraction using a power law model. The intensity at each pixel is then displayed (after normalization to 1 for convenience) to form a chemical map. Scale bar in a-d = 10 μm, in e (HRTEM images) = 10 nm, in e (SAED) = 51/nm, in f and i = 200 nm.

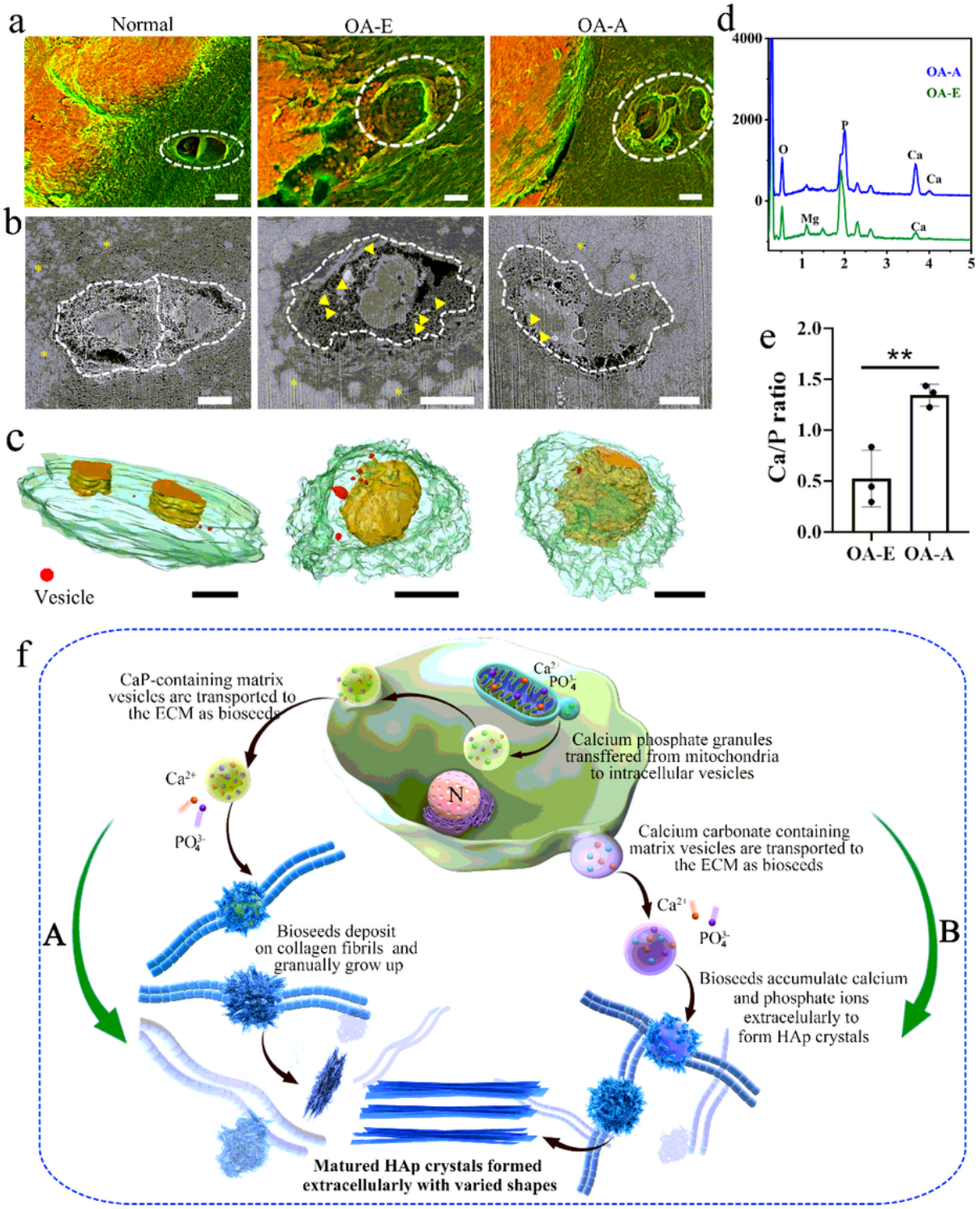


## Figure 4

**3D reconstruction of hypertrophic chondrocytes at calcified cartilage. (a).** DDC-SEM images showing the morphology of hypertrophic chondrocytes at the front of calcified cartilage region. **(b).** FIB-SEM slices revealing the corresponding chondrocyte lacunae environment of cartilage in early and advanced OA stages. Many calcium-rich vesicles (yellow arrowheads) were found in the lacunae of OA-A samples, and less of that was present in the lacunae of OA-E samples. Such vesicles were rarely observed in

chondrocyte lacunae of normal samples. **(c).** 3D reconstruction of lacunae (dark green) with hypertrophic chondrocytes (orange) and inner vesicles (red). **(d).** EDX spectra illustrating the calcium/phosphate-containing features of the vesicles in the lacunae of hypertrophic chondrocytes for OA-E and OA-A samples. **(e).** The calculated Ca/P ratios of matrix vesicles for OA-E and OA-A samples. P value = 0.0019 (**) **(f).** Schematic diagram showing the proposed cell-mediated extracellular mineral deposition process in OA. Ions or amorphous materials was transported via two kinds of matrix vesicles to the extracellular matrix in OA-E (right: A pathway) and OA-A (right: B pathway), acting as bioseeds and subsequently converting to more crystalline apatite. The matrix vesicles as bioseeds in OA-E are in green, and calcium carbonate-containing vesicles in OA-A are in purple. 'N' represents the cell nucleus. Calcium and phosphate ions are shown in orange and purple. The collagen-mediated mineralization process is depicted at the bottom with nuclei foci formation, sequential morphology transformation and mineral maturation. Scale bar, a = 10 μm, b and c = 4 μm.

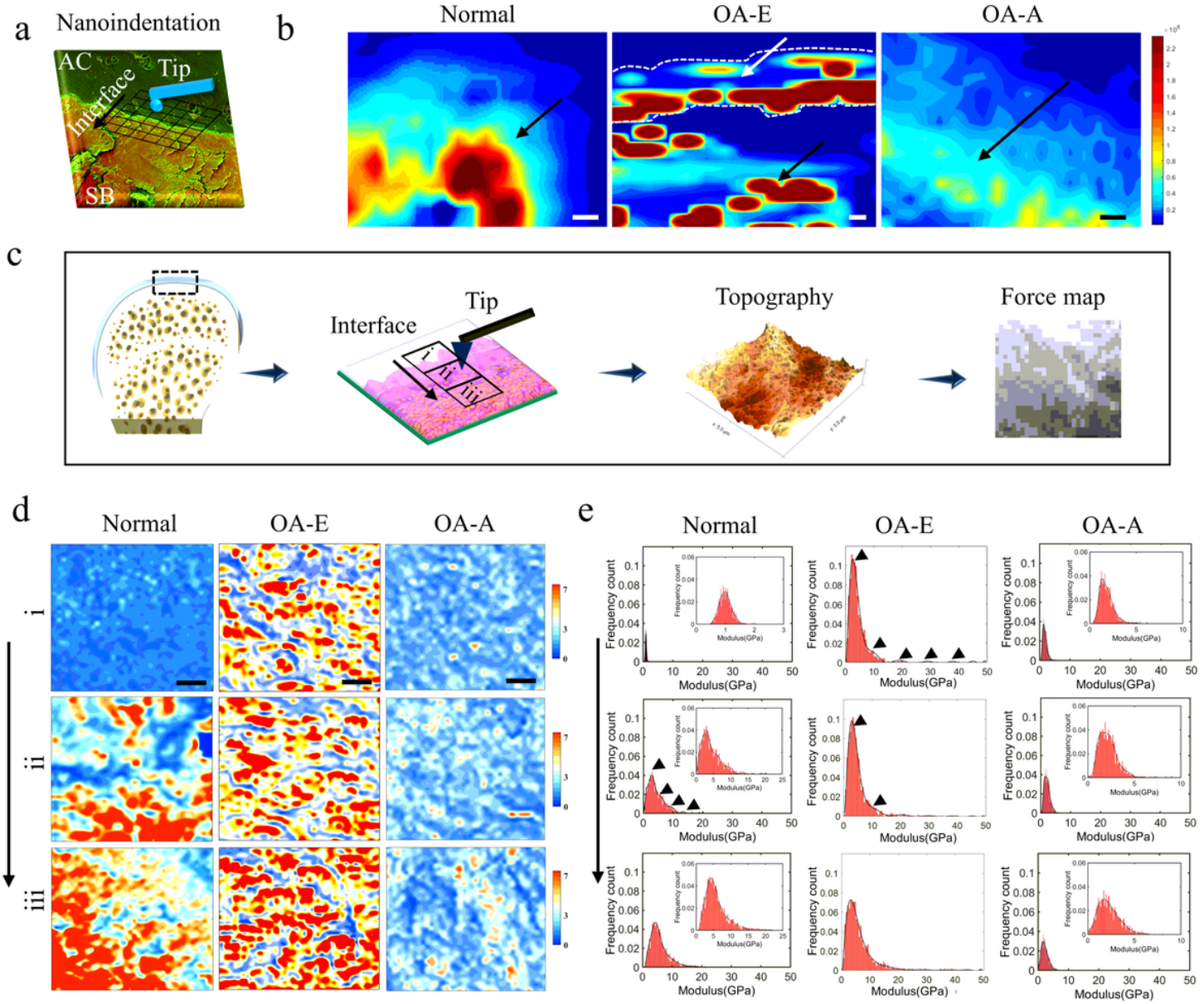

## Figure 5

**Correlating the local mechanical response of calcified cartilage tissues during OA progression. (a)**. Schematic diagram showing nanoindentation test for local calcified cartilage tissues of cartilage in OA progression (10×10 μm step). **(b)**. Efficient modulus map of the calcified cartilage tissues revealing increased and decreased local tissue modulus of OA-E and OA-A samples, compared with normal samples. White arrows indicated the duplicate calcified region overlying the original calcified cartilage (black arrows). **(c)**. Schematic diagram illustrating the test of nanomechanical response of calcified cartilage tissues from less mineralized region (i) to intermediate mineralized region(ii), and to the highly mineralized region (iii) using AFM (0.15×0.15 μm step). **(d)**. Consecutive AFM stiffness maps of selected regions in c (i, ii and iii) at calcified cartilage tissues for different samples. **(e)**. Corresponding stiffness distributions across calcified cartilage tissues for different samples. Scale bars in b= 20 μm, in d= 1 μm.

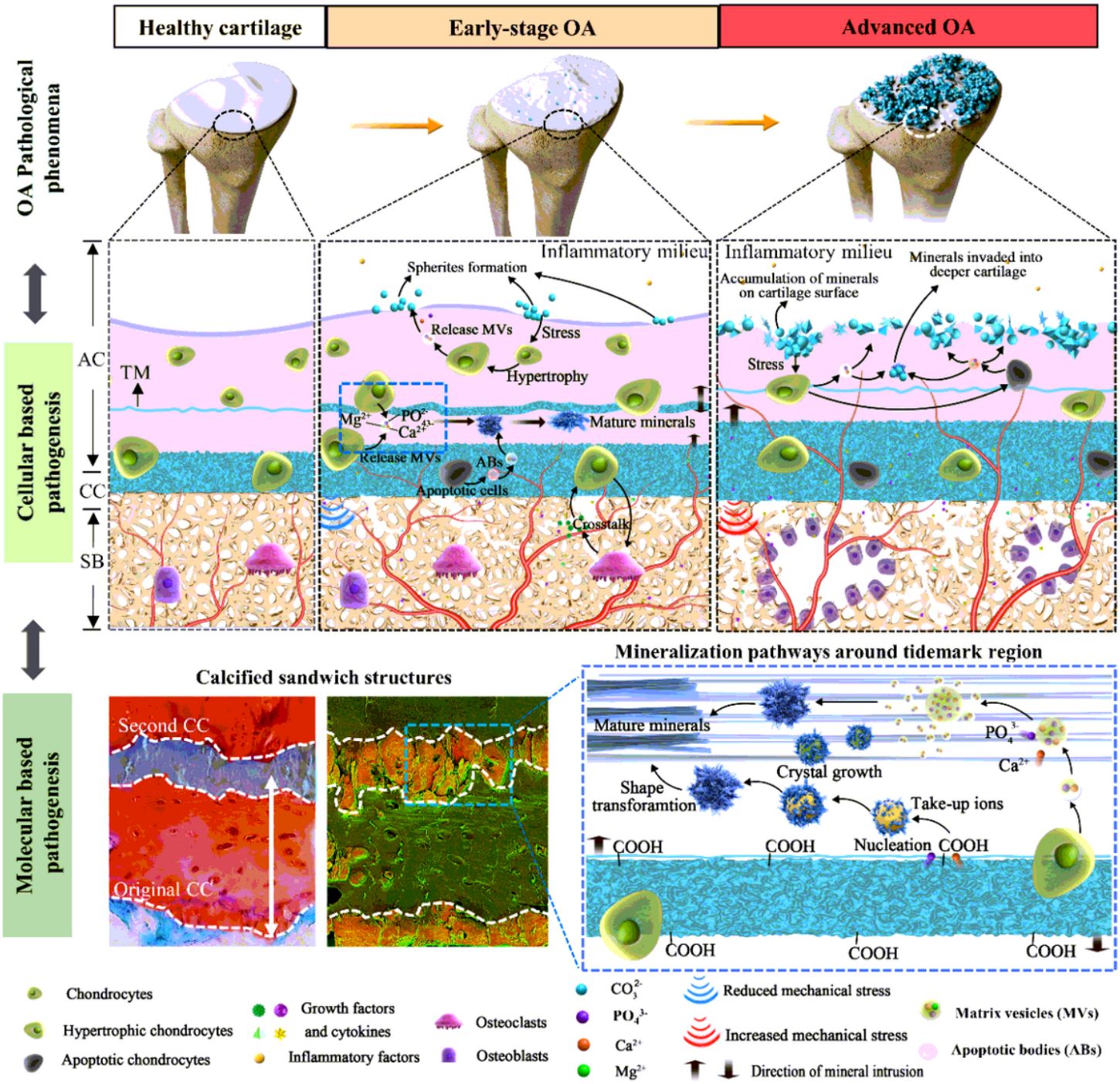


**Figure 6**

Schematic showing pathological calcification process at joint surface and osteochondral transitional region as OA processes.

# Supplementary Files

This is a list of supplementary files associated with this preprint. Click to download.

- SupplementalInformation.docx